Hindawi
Advances in Civil Engineering
Volume 2020, Article ID 6069432, 13 pages
https://doi.org/10.1155/2020/6069432

Research Article

Analysis of Support Reaction Curves considering Time-Varying Effect of Shotcrete

Ya-Qiong Wang[1] **and Ming-Rui Luo**[2]

[1]*Shaanxi Provincial Major Laboratory for Highway Bridge & Tunnel, School of Highway, Chang'an University, Xi'an 710064, China*
[2]*School of Highway, Chang'an University, Xi'an 710064, China*

Correspondence should be addressed to Ya-Qiong Wang; ys08@gl.chd.edu.cn

Received 11 September 2019; Revised 26 June 2020; Accepted 31 July 2020; Published 17 August 2020

Academic Editor: Dimitris Rizos

Copyright © 2020 Ya-Qiong Wang and Ming-Rui Luo. This is an open access article distributed under the Creative Commons Attribution License, which permits unrestricted use, distribution, and reproduction in any medium, provided the original work is properly cited.

The core content of the convergence constraint method is to determine the reasonable support time and support stiffness. The stiffness of shotcrete in supporting structure is dynamic. The support stiffness of shotcrete is roughly calculated in engineering, which results in a waste of materials and increases the risk of construction. Therefore, in this study, considering the time-varying characteristics of shotcrete, combined with the elastic-plastic theory and the space effect of excavation surface, the calculation equation describing the support reaction curve is given. An example is given to show that the stiffness of shotcrete considering time-varying effect is lower than that of shotcrete without time-varying effect, and the difference is the most obvious in the age of 0–3 days. However, in the later stage, the stiffness growth rate of shotcrete considering time-varying effect is higher than that of shotcrete without time-varying effect. This study can predict the whole process of the support reaction curve, which can make the application of the convergence constraint method in tunnel support design more accurate, and provide a theoretical basis for the design of supporting structure in the process of tunnel construction.

1. Introduction

With the development of the New Austrian Tunneling Method (NATM), the design concept of tunnel has changed greatly [1, 2]. The core of the New Austrian Tunneling Method is to give full play to the stability of the rock. From this point of view, the rock bears an important responsibility in the foundation-structure interaction system, which not only acts as the supporting part of the tunnel structure but also acts as a source of pressure on artificial support. The interaction between support and rock has always been the focus of research in the field of tunnel engineering, but there is still a lot of controversy about when to apply the supporting structure. The selection of supporting time is a key point in the total of tunnel supporting structure.

At present, the constraint convergence method (CCM) is the most commonly used method to study the interaction between support and rock. The core of the constrained convergence method is to determine the setting time and stiffness of the supporting structure to ensure that the supporting structure can reach equilibrium with the rock [3]. This process is shown in Figure 1, in which the abscissa is the radial displacement of the inner wall of the tunnel, the ordinate is the supporting force of the inner wall, and the starting point P_0 represents the original stress state before the tunnel excavation. After the tunnel excavation, the supporting force of the inner wall provided by the rock gradually decreases, and the rock has elastic deformation until point A. After point A, the rock has plastic deformation, and at this time, the growth of the radial displacement of the rock accelerates. Due to the continuous expansion of the plastic region, the relaxation pressure appears in the plastic zone, and the superposition results in the upward warping of the curve. This is the rock characteristic curve of the arch in the typical state of the soft stratum. If the strength of the rock is high, the plastic

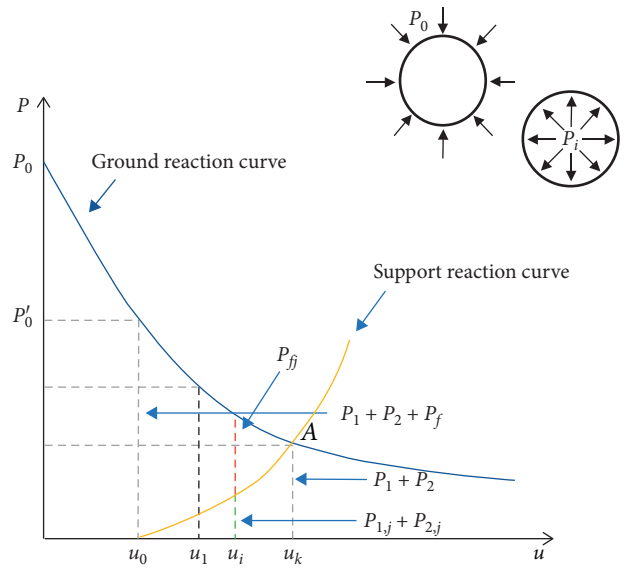

Figure 1: Ground reaction curve and suppose reaction curve.

deformation is not produced, or the plastic zone is small, and the relaxation pressure does not occur; the curve and warping will not occur. The tunnel support system begins to be set up after a certain distance of tunnel excavation, and its support reaction can be expressed by a curve, that is, SRC. The intersection of SRC and GRC is the expected support point, and the balance of SRC and GRC is reached.

The ground reaction curve was first put forward by Fenner [4]. According to the elastic-plastic theory, Fenner deduced the relationship between the radial displacement of tunnel wall and the rock pressure of tunnel. On this basis, scholars have made an in-depth study of the rock characteristic curve and obtained some conclusions. With the development and application of elastic-plastic theory, the research of support-rock has also been developed. The research shows that the support resistance is closely related to the plastic deformation of rock. So far, a variety of models have been established based on GRC and applied in foundation reinforcement, and so on [5–19].

Oreste explores the interaction between tunnel rock and support, adopts the concept of limit state, gives the SRC and calculation formula of main support forms, analyzes the combination of support forms, discusses the interaction between initial support and secondary lining, and gives the calculation method of composite lining [20]. The study shows that the bearing capacity of shotcrete increases with the excavation of the tunnel, and in the process of tunnel excavation, the excavation face of the tunnel will continue to move forward before the shotcrete support hardens completely [21]. At the same time, the supporting effect of tunnel excavation on rock began to disappear. At this time, shotcrete support is in the early stage of bearing load. In this stage, the strength and stiffness of shotcrete are increasing with time and may be destroyed before reaching the ultimate strength. This phenomenon is closely related to the time-varying characteristics of shotcrete. Because the tunnel support problem is statically indeterminate, the load acting on the support is directly related to the stiffness of the support. Therefore, it can be considered that GRC depends on the nature of the rock itself, the variation of the stiffness of shotcrete support with time, and the excavation rate of the tunnel excavation surface. Stille et al. pointed out that, if the load acting on shotcrete support increases with time, if it exceeds the strength of support, it will lead to the instability of support [22]. However, the conventional GRC does not take into account this effect on the early characteristics of shotcrete. At present, the above theory cannot reasonably explain the early failure of shotcrete supporting structure. The interaction between shotcrete and rock is lack of reasonable and effective theoretical analysis, so it is necessary to establish SRC model considering the time-varying characteristics of shotcrete, so as to find out a more appropriate time to support.

In this study, based on the Mohr–Coulomb criterion and the space effect of excavation surface, the calculation model of SRC considering the time-varying characteristics of shotcrete is put forward, and combined with the process of tunnel construction, the suggestion of selecting the time of support is given. This paper gives a new understanding of SRC in the early stage, in order to provide a new idea for the study of time-varying characteristics of shotcrete.

2. Time-Varying Characteristics of Shotcrete

As an important part of the initial support of the tunnel, shotcrete carries the load together with the rock since it is applied. Because this paper assumes that the tunnel is excavated at a uniform speed, and the stress release rate and the mechanical properties of shotcrete are related to time, for a certain analytical section, the load of shotcrete may be greater than its current ultimate bearing capacity, resulting in rock instability. This phenomenon should be paid attention to in the design of tunnel supporting structure.

Creep is an important time-varying characteristic of shotcrete. Creep refers to the phenomenon that the stress of concrete is constant and the action time of strain and load increases. It is generally believed that the factors affecting concrete creep are cement type, aggregate type, different water-cement ratio, admixture, loading age, loading stress, loading time, specimen size, and so on.

At present, scholars from various countries have done a lot of research on the creep performance of concrete. The study shows that the creep coefficient or degree of creep is an important parameter for calculating the constitutive relation of stress and strain of early age concrete. There are many factors that affect this parameter, and the expression is complex, so it is difficult to describe these two parameters exactly [23–47].

Therefore, scholars from various countries have put forward many mathematical calculation models of creep coefficient. Due to the different factors considered, the calculation formulas are also different, so there are two methods: one is to make the creep coefficient table in the form of the product of each partial coefficient, such as the representative ACI-209 model [48, 49] and GL2000 model [50], and the other is to make the creep coefficient table in the form of the sum of each partial coefficient, such as CEB-

FIP model [51] and B3 model [52, 53]. In order to verify which model has the best prediction effect, a large number of domestic and foreign scholars have done a large number of comparative experiments. The results show that, in terms of calculation accuracy, the prediction results of B3 model and GL2000 model are close to the measured values, and there is a big gap between the predicted results of the CEB-FIP model and ACI-209 model and the measured values [54–59]. From the point of view of the uniformity of the distribution of prediction results, the B3 model, GL2000 model, and CEB-FIP model perform better. In terms of the parameters considered, CEB-FIP focuses on strength and temperature, while the B3 model focuses on mix ratio.

More importantly, the CEB-FIP model is the most accurate in predicting Portland cement concrete. The CEB-FIP model adopts the creep coefficient expression of the superposition of elastic deformation and plastic deformation. This model is suitable for the creep calculation of concrete whose compressive stress does not exceed $0.5Ra$ and is suitable for tensile concrete. For shotcrete, the working environment and load distribution are analyzed and summarized, and the following conclusions are drawn:

(1) Generally speaking, shotcrete belongs to Portland concrete, and the creep law is consistent with that of ordinary concrete in qualitative analysis.

(2) The load on shotcrete is uncertain. According to statistics, the average radial contact stress of shotcrete is 297 kPa.

(3) The contact stress of shotcrete increases with time, and its internal stress increases gradually with time. The values of the two stresses finally tend to be stable, and their internal forces are mostly less than 0.5 Ra.

According to the above characteristics, the CEB-FIP model is used in this study, and its creep coefficient equation is

$$\varphi(t,\tau) = \beta_a(\tau) + \phi_d\beta_d(t-\tau) - \phi_f\left[\beta_f(t) - \beta_f(\tau)\right], \quad (1)$$

where $\varphi\ (t,\ \tau)$ is the creep deformation coefficient of shotcrete structure at t age, and the observation time is the creep deformation coefficient of τ. $\beta_a(\tau)$ is the irrecoverable deformation part produced at the initial stage of loading, $\beta_d(t-\tau)$ is the delayed elastic strain increasing with time, and ϕ_f is the flow plasticity coefficient.

For shotcrete, Bay and Stokoe II [60] used the sound wave method to obtain the relationship between elastic modulus and age of the shotcrete equation:

$$E(\tau) = E_0\left[1 - \alpha e^{-m\tau} - (1-\alpha)e^{-n\tau}\right], \quad (2)$$

where E_0 is the final elastic modulus of shotcrete, m and n values can be referred to [61, 62], and t is the age of shotcrete.

The parameters in equation (2) are often simply fitted according to the field measured data or selected according to the type of shotcrete. In this way, the time-varying characteristics of shotcrete are not taken into account. Therefore, in this study, the equivalent elastic modulus is introduced to improve the formula.

In creep theory, the ratio of creep strain to instantaneous elastic strain is creep coefficient $\varphi(t,\tau)$. At present, the international definition of creep coefficient can be summarized as follows:

$$\varepsilon_c(t,\tau) = \frac{\sigma(\tau)}{E_t}\varphi(t,\tau). \quad (3)$$

The creep coefficient has a negative correlation with the age t of concrete and a positive correlation with the time of concrete bearing load. However, with the increase of time, the growth rate of creep coefficient under the load of concrete will gradually decrease. Therefore, the age of concrete and the time of concrete bearing load are two important factors that determine the creep coefficient. Therefore, the creep function can be expressed as the following equation:

$$J(t,\tau) = \frac{1+\varphi(t,\tau)}{E(\tau)}. \quad (4)$$

Therefore, the equivalent elastic modulus of shotcrete can be obtained:

$$E_{\text{equ}}(\tau) = \frac{E(\tau)}{1+\varphi(t,\tau)}, \quad (5)$$

where E_{equ} is the equivalent elastic modulus of shotcrete.

3. Space Effect of Excavation Face

The safety of the steel frame and shotcrete structure in the initial support is very important to the safety of tunnel construction, and their stress is the key to tunnel design [63–69]. Due to the characteristics of shotcrete, in the time when it reaches the design strength, the longitudinal advance of the excavation face produces displacement release, which leads to a certain difference between the supporting load growth law and the steel frame. Therefore, in order to accurately evaluate the supporting effect, the changing characteristics of the supporting structure must be comprehensively considered. The calculation model is shown in Figure 2, and the derivation process is based on the following assumptions:

(1) The rock is a homogeneous and isotropic elastic-plastic rock mass

(2) The rock satisfies the Mohr–Coulomb yield criterion

(3) The deep-buried circular tunnel is infinitely long

(4) According to the plane problem, the compressive stress is positive, the tensile stress is negative, and the direction of tunnel excavation is positive

3.1. Virtual Support Force. Tunnel excavation is essentially a three-dimensional problem, and the excavation surface shows a constraint in the direction of both the vertical section and the cross-section [70]. The coupling effect caused by the constraint in different directions has a certain limiting effect on the displacement of the rock around the cave, so that the elastic-plastic deformation of the rock cannot be released immediately in a certain range near the excavation

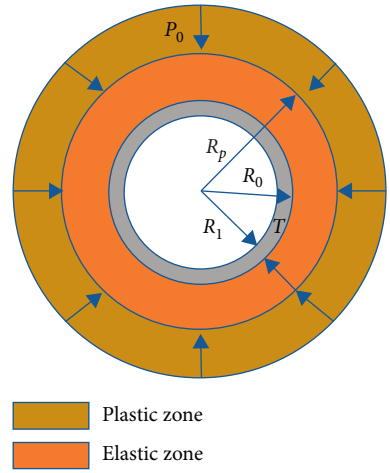

Figure 2: Circular tunnel model in hydrostatic pressure field.

face, so as to maintain its own stability to a certain extent. The constraint action is generally composed of rock pressure, space effect of excavation face, and support resistance.

In order to analyze the abstract space constraint effect of the tunnel excavation surface with the equivalent plane strain problem, a concept called "virtual supporting force" is introduced [71]. Its physical meaning is that it is considered to take a section near the tunnel excavation surface for analysis, which is called the plane section, which is called the analysis section. After the analysis section is removed, it will continue to converge, but due to the effect between empty excavation surfaces, the application of radial force on the cross-section wall will prevent the trend of continuous deformation of the analysis section, which is called virtual supporting force. As shown in Figure 3, the virtual supporting force gradually decreases with the increase of the distance between the analysis section and the excavation surface, and the virtual supporting force reaches the maximum value on the palm face. The study shows that the release formula of rock pressure is equation (6) [72]. At the moment of tunnel excavation, it can be considered that the rock pressure has been released by 30%. Therefore, the virtual supporting force will not be equal to P_0 in numerical value, and the constraint P_i can be expressed as equation (8).

Based on the maximum radius of the plastic zone of rock, Vlachopoulos and Diederichs [73] put forward the expression of displacement release coefficient of ideal elastic-plastic rock. Alejano et al. [74] extended and analyzed it through numerical simulation and pointed out that it is also suitable for strain-softened rock, and the calculation method of relevant parameters is given through statistical analysis. In this study, the characteristic curve of supporting structure is deduced based on the Vlachopoulos formula equation:

$$\frac{u_{R_0}}{u_{\max}} = \begin{cases} u_{\max}\dfrac{1}{3}e^{-\left(3R_p/20R_0\right)}e^{\left(x/R_0\right)}, & x < 0, \\ 1-\left(1-u_{\max}\dfrac{1}{3}e^{-\left(3R_p/20R_0\right)}\right)e^{-\left(3x/2R_p\right)}, & x \geq 0, \end{cases} \tag{6}$$

where u_{R_0} is the radial displacement of tunnel excavation face, R_p is the maximum radius of the plastic zone without support, $u_{\max}$ is the maximum short-term radial displacement distant from the face and corresponding to plane strain analysis of a tunnel cross section, P_0 is the initial rock pressure, x is the distance between the analysis section of the tunnel and the excavation face, and R_0 is the tunnel radius.

3.2. The Elastic Solution. According to the thick-walled cylinder theory, the elastic convergence equation of the radial displacement of the tunnel rock without support can be obtained:

$$u_{R_0} = \frac{1+\mu}{E}R_0\left(P_0 - P_f\right), \tag{7}$$

where u_{R_0} is the radial displacement of the tunnel, μ is Poisson's ratio of rock, E is the elastic modulus of rock, and P_i is the supporting force acting on the rock:

$$P_f = P_0 - \frac{Eu_{R_0}}{(1+\mu)R_0}. \tag{8}$$

By combining equations (6)–(8), P_f under elastic conditions can be obtained:

$$P_f = \begin{cases} P_0 - \dfrac{Eu_{\max}(1/3)e^{-\left(3R_p/20R_0\right)}e^{\left(x/R_0\right)}}{(1+\mu)R_0}, & (x < 0), \\ P_0 - \dfrac{Eu_{\max}\left[1-\left(1-u_{\max}(1/3)e^{-\left(3R_p/20R_0\right)}\right)e^{-\left(3x/2R_p\right)}\right]}{(1+\mu)R_0}, & (x \geq 0). \end{cases} \tag{9}$$

3.3. The Plastic Solution. In infinite media, the elastic-plastic solution of the circular hole problem is obtained by using the Mohr–Coulomb criterion and the unrelated flow rule.

Equation (10) can be obtained from the Mohr–Coulomb yield criterion:

$$\tau_n = \sigma_n \tan\varphi + c, \tag{10}$$

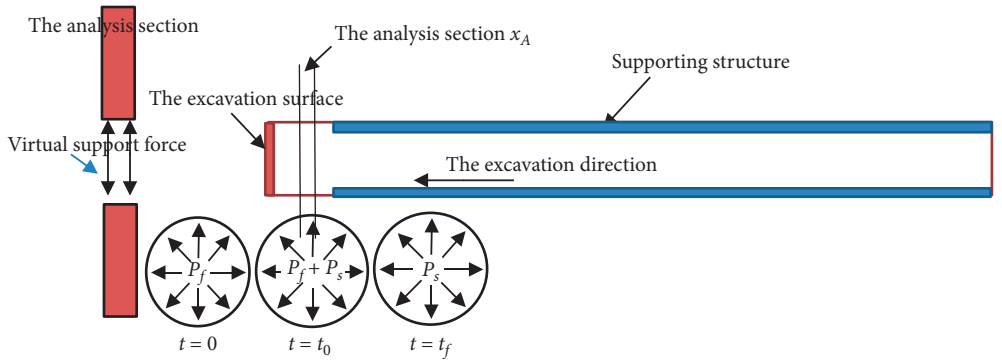

Figure 3: Diagram of virtual support force.

where σ_n and τ_n are the normal stress and tangential stress on the failure surface, φ is the internal friction angle of the rock, and c is the cohesion of the rock.

In this study, according to the previous assumptions, the Mohr–Coulomb yield criterion can be written as the following equation:

$$\sigma_\theta^p = \frac{1+\sin\varphi}{1-\sin\varphi}\sigma_r^p - \frac{2\cos\varphi}{1-\sin\varphi}c, \tag{11}$$

where σ_θ^p is the tangential stress of the plastic zone rock and σ_r^p is the radial stress of the plastic zone rock.

The equilibrium differential equation can be written as the following equation:

$$\frac{\mathrm{d}\sigma_r^p}{\mathrm{d}r} + \frac{\sigma_r^p - \sigma_\theta^p}{r} = 0. \tag{12}$$

With the combination of equations (11) and (12) and considering the boundary condition $r = R_0$ and the late $\sigma_r^p = P_i$, the lateral pressure coefficient is 1 and the tangential stress component and radial stress component of the plastic zone of rock can be obtained:

$$\begin{cases} \varepsilon_r^p = \left(P_f + c\cot\varphi\right)\left(\dfrac{r}{R_0}\right)^{(2\sin\varphi/(1-\sin\varphi))} - c\cot\varphi, \\ \varepsilon_\theta^p = \left(P_f + c\cot\varphi\right)\left(\dfrac{1+\sin\varphi}{1-\sin\varphi}\right)\left(\dfrac{r}{R_0}\right)^{(2\sin\varphi/(1-\sin\varphi))} - c\cot\varphi. \end{cases} \tag{13}$$

On the elastic-plastic interface, the stress in the plastic zone is balanced with that in the elastic zone:

$$\begin{aligned} \sigma_r^e &= \sigma_r^p, \\ \sigma_\theta^e &= \sigma_\theta^p. \end{aligned} \tag{14}$$

At this time, the stress on the interface of the elastic-plastic zone should satisfy both the elastic condition and the plastic condition, and the elastic condition is

$$\sigma_r^e + \sigma_\theta^e = 2P_0. \tag{15}$$

With the combination of equations (11) and (15), in $r = R_p$, the plastic condition can be expressed as

$$\begin{cases} \sigma_r^p = P_0(1-\sin\varphi) - c\cos\varphi, \\ \sigma_\theta^p = P_0(1+\sin\varphi + c\cos\varphi. \end{cases} \tag{16}$$

R_p can be obtained by combining equations (13) and (16):

$$R_p = R_0\left[(1-\sin\varphi)\frac{P_0 + c\cot\varphi}{P_f + c\cot\varphi}\right]^{((1-\sin\varphi)/2\sin\varphi)}. \tag{17}$$

At this time, the rock outside the radius of the plastic zone R_p is still in the elastic state, and the boundary condition is

$$\begin{aligned} r &= \infty, \\ \sigma_r^e &= P_0. \end{aligned} \tag{18}$$

At $r = R_p$,

$$\sigma_r^e = \sigma_r^p = c\cot\varphi\left[\left(\frac{R_p}{R_0}\right)^{(2\sin\varphi/(1-\sin\varphi))} - 1\right]. \tag{19}$$

According to the geometric equation of axisymmetric plane strain state equation,

$$\begin{aligned} \varepsilon_r &= \frac{\mathrm{d}u}{\mathrm{d}r}, \\ \varepsilon_\theta &= \frac{u}{r}. \end{aligned} \tag{20}$$

Combining equations (12)–(20),

$$\begin{cases} \sigma_r^e = P_0 - \dfrac{R_p^2}{r^2}\left(P_0 - c\cot\varphi\left[\left(\dfrac{R_p}{R_0}\right)^{(2\sin\varphi/(1-\sin\varphi))} - 1\right]\right), \\ \sigma_\theta^p = P_0 + \dfrac{R_p^2}{r^2}\left(P_0 - c\cot\varphi\left[\left(\dfrac{R_p}{R_0}\right)^{(2\sin\varphi/(1-\sin\varphi))} - 1\right]\right), \\ u^e = \dfrac{(1+\mu)R_p^2}{Er}\left(P_0 - c\cot\varphi\left[\left(\dfrac{R_p}{r}\right)^{(2\sin\varphi/(1-\sin\varphi))} - 1\right]\right). \end{cases} \tag{21}$$

In order to obtain the displacement u^p of rock plastic zone, it can be assumed that the volume of rock plastic zone is constant in the case of small deformation:

$$\varepsilon_r^p + \varepsilon_\theta^p + \varepsilon_z^p = 0. \tag{22}$$

Geometric equations of the axisymmetric plane strain state are as follows:

$$\begin{aligned} \varepsilon_r &= \frac{\mathrm{d}u}{\mathrm{d}r}, \\ \varepsilon_\theta &= \frac{u}{r}, \\ \varepsilon_z &= 0. \end{aligned} \tag{23}$$

The calculation of elastic displacement is the same as that in the elastic-plastic state:

$$u^p = \frac{(1+\mu)R_p^2}{Er}\left(P_0 - c\cot\varphi\left[\left(\frac{R_p}{r}\right)^{(2\sin\varphi/(1-\sin\varphi))} - 1\right]\right). \tag{24}$$

When $r = R_0$, the radial displacement under the action of P_f can be calculated by combining equations (16), (17), and (24):

$$u_{R_0}^{P_f} = \frac{(1+\mu)R_0}{E}\left(P_0\sin\varphi + c\cos\varphi\right)\left[(1-\sin\varphi)\frac{P_0 + c\cot\varphi}{P_f + c\cot\varphi}\right]^{((1-\sin\varphi)/\sin\varphi)}. \tag{25}$$

Thus,

$$P_f = \frac{(1+\mu)(1-\sin\varphi)\left(P_0 + c\cot\varphi\right)}{\left(Eu_{R_0}^{P_f}/R_0\left(P_0\sin\varphi + c\cos\varphi\right)\right)^{(\sin\varphi/(1-\sin\varphi))}} - c\cot\varphi. \tag{26}$$

The combination of equations (6) and (26) can be obtained:

$$P_f = \begin{cases} \dfrac{(1+\mu)(1-\sin\varphi)\left(P_0 + c\cot\varphi\right)}{\left(Eu_{\max}^2(1/3)e^{-\left(3R_p/20R_0\right)}e^{\left(x/R_0\right)}/R_0\left(P_0\sin\varphi + c\cos\varphi\right)\right)^{(\sin\varphi/(1-\sin\varphi))}} - c\cot\varphi, & (x<0), \\ \dfrac{(1+\mu)(1-\sin\varphi)\left(P_0 + c\cot\varphi\right)}{\left(Eu_{\max}\left(1-\left(1-u_{\max}(1/3)e^{-\left(3R_p/20R_0\right)}\right)e^{-\left(3x/2R_p\right)}\right)/R_0\left(P_0\sin\varphi + c\cos\varphi\right)\right)^{(\sin\varphi/(1-\sin\varphi))}} - c\cot\varphi, & (x\geq 0). \end{cases} \tag{27}$$

4. Construction of SRC

4.1. The Elastic Solution. In this study, it is assumed that the rock and the supporting structure satisfy the continuity assumption, the supporting structure and the rock are closely connected, and there is no relative displacement.

According to equations (7) and (8), (28) can be obtained when only elastic displacement occurs in rock:

$$u_{R_0}^{P_i} = \frac{1+\mu}{E}R_0\left(P_0 - P_i\right). \tag{28}$$

The supporting resistance caused by supporting structure is P_s:

$$\begin{cases} P_s = \dfrac{K_s}{R_0}u_{R_0}^{P_s}, \\ u_{R_0}^{P_s} = u_{R_0}^{P_i} - u\left(x_A\right), \end{cases} \tag{29}$$

where K_s is the stiffness of the supporting structure and x_A is the analysis section:

$$\frac{u_{R_0}(x_A)}{u_{\max}} = \begin{cases} u_{\max}\dfrac{1}{3}e^{-\left(3R_p/20R_0\right)}e^{\left(x_A/R_0\right)}, & (x_A<0), \\ 1-\left(1-u_{\max}\dfrac{1}{3}e^{-\left(3R_p/20R_0\right)}\right)e^{-\left(3x_A/2R_p\right)}, & (x_A\geq 0). \end{cases} \tag{30}$$

The radial displacement of tunnel face under the action of P_i can be obtained by combining equations (8), (9), (28), and (29):

$$u_{R_0}^{P_i} = \begin{cases} \dfrac{(1+\mu)R_0}{E}\left[-\dfrac{K_s}{R_0}u_{R_0}^{P_i} + \dfrac{K_s}{R_0}u_{R_0}(x_A) + \dfrac{Eu_{\max}(1/3)e^{-\left(3R_p/20R_0\right)}e^{\left(x/R_0\right)}}{(1+\mu)R_0}\right], & (x<0), \\ \dfrac{(1+\mu)R_0}{E}\left[-\dfrac{K_s}{R_0}u_{R_0}^{P_i} + \dfrac{K_s}{R_0}u_{R_0}(x_A) + \dfrac{Eu_{\max}\left[1-\left(1-u_{\max}(1/3)e^{-\left(3R_p/20R_0\right)}\right)e^{-\left(3x/2R_P\right)}\right]}{(1+\mu)R_0}\right], & (x\geq 0). \end{cases} \tag{31}$$

4.2. The Plastic Solution. According to the corollary in Section 3.3, the radial displacement of tunnel excavation surface under the action of P_i is

$$u_{R_0}^{P_i} = \frac{(1+\mu)R_0}{E}\left(P_0\sin\varphi + c\cos\varphi\right)\left[(1-\sin\varphi)\frac{P_0 + c\cot\varphi}{P_i + c\cot\varphi}\right]^{((1-\sin\varphi)/\sin\varphi)}. \tag{32}$$

The radial displacement of tunnel face under the action of P_i can be obtained by combining equations (8), (9), (29), and (32):

$$\frac{u_{R_0}^{P_i}E}{(1+\mu)R_0} = \begin{cases} \left(P_0\sin\varphi + c\cos\varphi\right)\left[(1-\sin\varphi)\dfrac{P_0+c\cot\varphi}{\left(K_s/R_0\right)u_{R_0}^{P_s} + P_0 - \left(Eu_{\max}(1/3)e^{-\left(3R_p/20R_0\right)}e^{\left(x/R_0\right)}/(1+\mu)R_0\right) + c\cot\varphi}\right]^{((1-\sin\varphi)/\sin\varphi)}, & (x<0), \\ \left(P_0\sin\varphi + c\cos\varphi\right)\left[(1-\sin\varphi)\dfrac{P_0+c\cot\varphi}{\left(K_s/R_0\right)u_{R_0}^{P_s} + P_0 - \left(Eu_{\max}\left[1-\left(1-u_{\max}(1/3)e^{-\left(3R_p/20R_0\right)}\right)e^{-\left(3x/2R_P\right)}\right]/(1+\mu)R_0\right) + c\cot\varphi}\right]^{((1-\sin\varphi)/\sin\varphi)}, & (x\geq 0). \end{cases} \tag{33}$$

4.3. Calculation of Support Stiffness. In this study, the equivalent stiffness of the supporting structure is calculated by using the research results of Oreste [20]. The equivalent stiffness of shotcrete can be calculated by

$$K_{\text{shot}} = \frac{E_{\text{equ}}(t)\left(R_0^2 - R_1^2\right)}{\left(1+\mu_s\right)\left[(1-2\mu_s)R_0^2 + R_1^2\right]R_0}, \tag{34}$$

where μ_s is shotcrete Poisson's ratio and R_1 is the inner diameter of the tunnel after the injection of shotcrete.

The maximum supporting force produced by shotcrete can be calculated by

$$P_{\max,\text{shot}} = \frac{\sigma_{\text{shot},c}}{2}\left[1 - \frac{R_1^2}{R_0^2}\right], \tag{35}$$

where $\sigma_{\text{shot},c}$ is the uniaxial strength of the shotcrete.

The maximum displacement of shotcrete can be calculated by

$$u_{\max,\text{shot}} \cong u_{e,\text{shot}} + \varepsilon_{\text{br,con}}R_1 - \frac{2R_0R_1\left(1-\mu_s\right)}{(1-2\mu_s)R_0^2 + R_1^2}\frac{P_{\max,\text{shot}}}{K_{\text{shot}}}, \tag{36}$$

where $u_{\max,\text{shot}}$ is the maximum displacement that the shotcrete can bear, $u_{e,\text{shot}}$ is the maximum displacement in the elastic state of the shotcrete, and $\varepsilon_{\text{br,con}}$ is the failure strain of the shotcrete.

The equivalent stiffness of the steel arch frame can be calculated by

$$K_{\text{set}} = \frac{E_{\text{st}}A_{\text{st}}}{d\left(R_0 - \left(h_{\text{set}}/2\right)\right)^2}, \tag{37}$$

where K_{set} is the stiffness of the steel set; E_{st} is the elastic modulus for the steel; d is the steel set spacing along the tunnel axis; A_{st} is the cross-sectional area of the steel set section; and h_{set} is the cross-sectional height of the steel section.

The equilibrium condition gives (equation (38)) the maximum pressure p sustainable from the steel set:

$$P_{\max,\text{set}} \cong \frac{\sigma_{\text{st},y}A_{\text{set}}}{\left(R_0 - \left(h_{\text{set}}/2\right)\right)d}, \tag{38}$$

where $\sigma_{\text{st},y}$ is the yield strength of the steel.

The maximum displacement of the steel arch can be calculated by

$$u_{\max,\text{set}} = u_{\text{in,set}} + \varepsilon_{\text{br,set}}\left(R_0 - \frac{h_{\text{set}}}{2}\right), \tag{39}$$

where $u_{\max,\text{set}}$ is the maximum displacement that the steel arch frame can bear, $u_{\text{in,set}}$ is the displacement value during

the installation of the steel arch frame, and $\varepsilon_{br,set}$ is the failure strain of the steel arch frame.

As for radial anchored bolts, it results that

$$K_{bol} = \frac{1}{S_c S_l \left(\left(4L_{bol}/\pi\phi^2 E_{bol}\right) + Q\right)},$$

$$u_{max,bol} \cong u_{in,bol} + L_{bol}\left(\varepsilon_{br,bol} - \frac{4T_0}{\pi\phi^2 E_{bol}}\right), \tag{40}$$

$$P_{max,bol} = \frac{T_{max}}{S_c S_l},$$

where Q is the load-deformation constant for the anchor and head [75]; S_c and S_l are the circumferential spacing and longitudinal spacing; L_{bol} is the bolt length; ϕ is the bolt diameter; and E_{bol} is the elastic modulus for the steel; and T_{max} is the force that induces yielding of the steel.

For the composite supporting structure composed of shotcrete lining, steel bracing, and anchor, the stiffness, maximum bearing capacity, and maximum displacement of the composite supporting structure are expressed by

$$\begin{cases} K_{tot} = \sum_j K_j, \\ P_{max,tot} = \sum_j P_{max,j}, \\ u_{max,tot} = \min\left(u_{max,j}\right), \end{cases} \tag{41}$$

where K_{tot} is the total stiffness of the support system; $P_{max,tot}$ is the total pressure of the support system; $u_{max,tot}$ is the total displacement of the support system; K_j is the single support stiffness; $P_{max,j}$ is the single support pressure; and $u_{max,j}$ is the single support displacement.

5. Example and Analysis

The radius of a tunnel is 5m, the thickness of shotcrete is 0.2 m, the buried depth is 100m, and the relative humidity in the tunnel is 70%. The tunnel rock is grade IV, and the specific parameters of the rock are shown in Table 1. The parameters of the steel arch are shown in Table 2.

5.1. Calculation of Parameters of Shotcrete. In this study, C30 shotcrete (experimental data are taken from a certain section of tunnel), $\mu_{shot} = 0.2$. According to the variation of C30 elastic modulus with time, the fitting formula can be obtained:

$$E(\tau) = 38.03 \times \left(1 - 0.4797e^{-1.583\tau} - 0.5203e^{-0.07351\tau}\right). \tag{42}$$

The creep coefficient can be calculated by equation (1). According to the study [76], equation (1) can be fitted to synthesize equation (43), and the selection of parameters is shown in Tables 3–5:

$$\varphi(t,\tau) = \beta_a(\tau) + \sum_{i=1}^{4} C_i(\tau)\left[1 - e^{-q_i(t-\tau)}\right] + 0.108, \tag{43}$$

Table 1: Calculation parameters of surrounding rock.

E (GPa)	μ	γ (kN/m)	c (MPa)	φ (°)
2	0.3	20	18	27

Table 2: Calculation parameters of the steel frame.

E_{set} (GPa)	μ_{st}	A_{st} (cm^2)	h (cm)	d (cm)	σ_{st} (MPa)
210	0.3	35.5	20	80	215

where

$$\begin{cases} \beta_a(\tau) = 0.8\left[1 - \frac{1}{1.276}\left(\frac{\tau}{4.2 + 0.85\tau}\right)^{1.5}\right], \\ C_1(\tau) = 0.172, \\ q_1 = 0.0036, \\ C_2(\tau) = 0.12, \\ q_2 = 0.0046, \\ C_3(\tau) = C \times \varphi_f e^{-q_3(t-\tau)}, \\ C_4(\tau) = D \times \varphi_f e^{-q_4(t-\tau)}, \\ \varphi_f = \varphi_{f1}\varphi_{f2}, \\ \varphi_{f2} = \begin{cases} ah^2 + bh + c\,(h \le 1300), \\ 1.12\,(h > 1300), \end{cases} \\ h = 2\lambda\left(R_0 - R_1\right). \end{cases} \tag{44}$$

After selecting the parameters, combined with equations (41) and (42),

$$\begin{aligned} \varphi(t,\tau) = {} & 0.8\left[1 - \frac{1}{1.276}\left(\frac{\tau}{4.2 + 0.85\tau}\right)^{1.5}\right] \\ & + 0.172\left[1 - e^{-0.0036(t-\tau)}\right] + 0.12\left[1 - e^{-0.0046(t-\tau)}\right] \\ & + 0.832e^{-0.0365(\tau-3)}\left[1 - e^{-0.0365(t-\tau)}\right] \\ & + 1.482e^{-0.00075(\tau-3)}\left[1 - e^{-0.00075(t-\tau)}\right] + 0.108. \end{aligned} \tag{45}$$

5.2. Equivalent Elastic Modulus of Shotcrete. Combine equations (5), (42), and (45). In equation (45), $t = 28$. The equivalent elastic modulus of shotcrete can be obtained at different loading times, as shown in Table 6.

Table 3: Creep coefficient.

Relative humidity (%)	Coefficient	
	φ_1	λ
100	0.8	30.0
90	1.0	5.0
70	2.0	1.5
40	3.0	1.0

Table 4: The coefficient of a, b, and c.

Coefficient	h (mm)		
	$h \leq 200$	$200 < h \leq 900$	$900 < h \leq 1300$
a	1.00×10^{-5}	6.250×10^{-7}	-2.03×10^{-7}
b	-4.5×10^{-3}	-1.125×10^{-3}	1.875×10^{-4}
c	2.05	1.75	1.240

Table 5: The coefficient of C, D, q_3, and q_4.

Coefficient	h (mm)					
	<50	100	200	400	800	>1600
C	0.50	0.47	0.41	0.35	0.29	0.20
D	0.39	0.42	0.48	0.54	0.60	0.69
q_3	0.033	0.0335	0.034	0.035	0.038	0.05
q_4	0.0015	0.0013	0.0011	0.00085	0.00065	0.00053

Table 6: The time effect parameters of shotcrete.

Time (d)	Elastic modulus (GPa)	Creep coefficient	Equivalent modulus of elasticity (GPa)
0.25	6.32	1.55	2.48
0.5	10.69	1.52	4.24
0.75	13.74	1.50	5.50
1	15.90	1.47	6.43
1.25	17.46	1.45	7.13
1.5	18.61	1.42	7.69
1.75	19.49	1.40	8.13
2	20.18	1.37	8.51
2.25	20.74	1.35	8.84
2.5	21.22	1.32	9.14
2.75	21.63	1.30	9.41
4	23.25	1.19	10.62
7	26.20	0.98	13.23
14	30.96	0.65	18.72
20	33.48	0.46	22.86

As shown in Figure 4, regardless of whether the time effect is taken into account or not, the elastic modulus increases with the increase of time. However, in the initial stage, $E(\tau)$ is obviously higher than $E_{\text{equ}}(\tau)$, especially in 0–3 days, and the growth rate of $E(\tau)$ is also faster than that of $E_{\text{equ}}(\tau)$. However, with the increase of time, the creep coefficient is decreasing, and $E_{\text{equ}}(\tau)$ still keeps growing rapidly. The growth of $E(\tau)$ tends to be flat.

As shown in Figure 5, with the increase of time and the decrease of creep coefficient, both $E(\tau)$ and $E_{\text{equ}}(\tau)$ increase. Comparing the two figures, we can see that $E(\tau)$ will reach the standard of tunnel design earlier, but in fact, after considering the time effect of shotcrete, Figure 5(b) shows that the actual elastic modulus of shotcrete does not meet the standard of tunnel design. If the tunnel design is considered according to Figure 5(a), the shotcrete lining structure will be subjected to higher rock pressure prematurely, which may lay hidden dangers for future construction or operation. If the tunnel design is considered according to Figure 5(b), the actual strength of the shotcrete lining structure can be achieved when it is set. According to this design, the shotcrete lining structure can be set at the minimum rock pressure, which can improve the material utilization rate and reduce the safety risks.

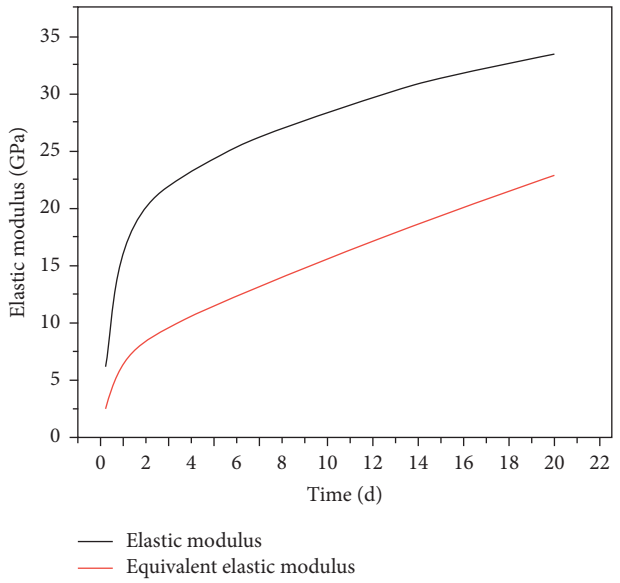

Figure 4: Modulus of elasticity of shotcrete.

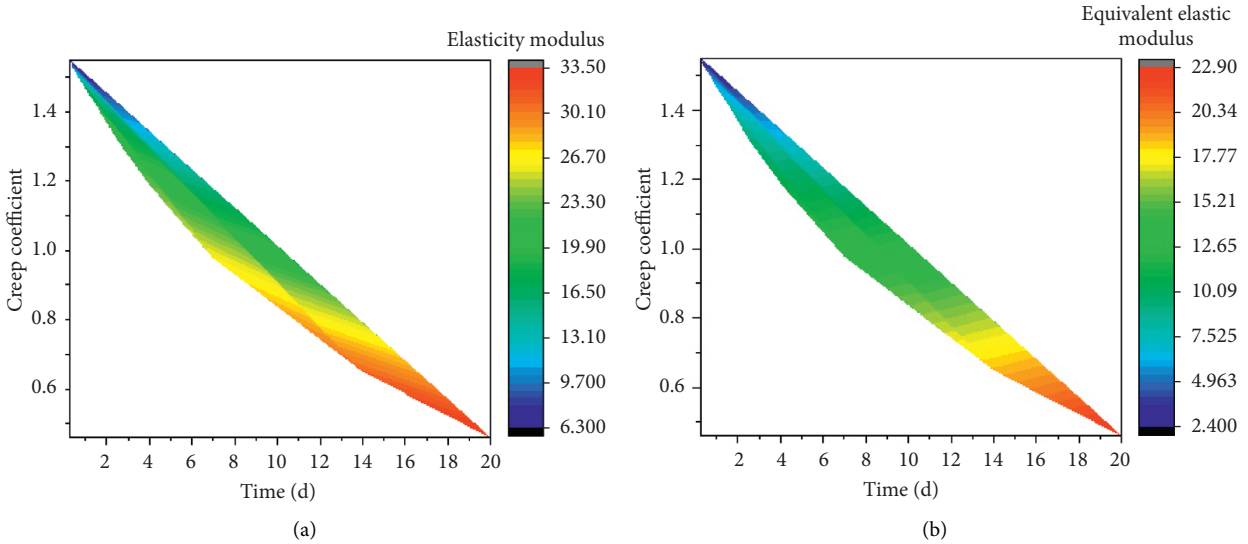

Figure 5: Relation diagram of elastic modulus, creep coefficient, and age.

Table 7: Stiffness of supporting structure.

Time (d)	$K_{shot,without}$ (GPa/m)	$K_{shot,equ}$ (GPa/m)	$K_{tot,without}$ (GPa/m)	$K_{tot,equ}$ (GPa/m)
0.25	0.054	0.021	0.093	0.060
0.5	0.092	0.036	0.131	0.075
0.75	0.118	0.047	0.157	0.086
1	0.137	0.055	0.175	0.094
1.25	0.150	0.061	0.189	0.100
1.5	0.160	0.066	0.199	0.105
1.75	0.167	0.070	0.206	0.109
2	0.173	0.073	0.212	0.112
2.25	0.178	0.076	0.217	0.115
2.5	0.182	0.078	0.221	0.117
2.75	0.186	0.081	0.225	0.120
4	0.200	0.091	0.238	0.130
7	0.225	0.114	0.264	0.152
14	0.266	0.161	0.305	0.200
20	0.288	0.196	0.326	0.235

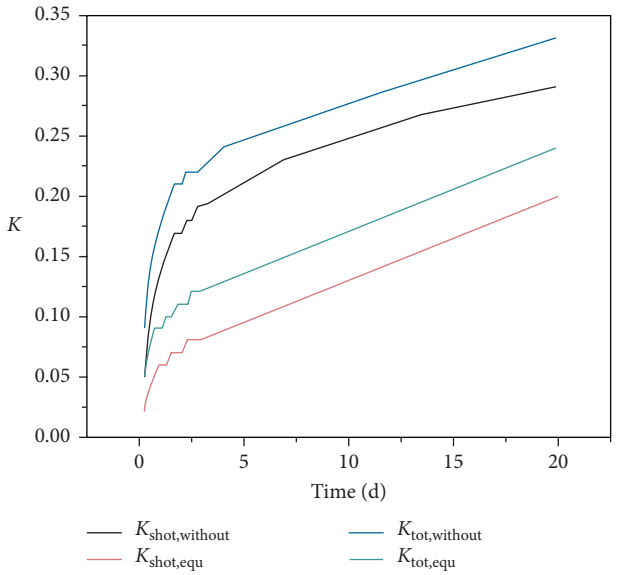

Figure 6: Stiffness comparison diagram.

5.3. Stiffness of Supporting Structure. The stiffness of shotcrete can be calculated by equation (34), and the stiffness of steel arch can be calculated by equation (37), $K_{set} = 0.388$ GPa/m. The stiffness of the supporting structure can be calculated by equation (41), and the calculated results are shown in Table 7. The support stiffness without considering the time effect is denoted as $K_{without}$, and the support stiffness after considering the time effect is equivalent support stiffness.

It can be seen that when the time effect of shotcrete is not taken into account, the value of $K_{tot,without}$ is almost twice that of $K_{tot,equ}$ in the age of 0–2 days. With the increase of time, the creep coefficient decreases gradually, the growth rate of $K_{tot,equ}$ gradually accelerates, while the growth rate of $K_{tot,\ without}$ gradually slows down. Therefore, the supporting force of shotcrete structure with $K_{tot,equ}$ is less than that of shotcrete structure with $K_{tot,\ without}$ under the same time and displacement. (as shown in Figure 6)

6. Conclusions

In this study, combined with the space effect of excavation surface and the time-varying characteristics of shotcrete, the calculation model of SRC is improved.

An example is given to compare the difference between considering and not considering the time-varying characteristics of shotcrete. The results show that when the time-varying characteristics of shotcrete are not considered, the elastic modulus and stiffness of shotcrete are higher than those without time-varying characteristics, and in the initial stage of the setting of the supporting structure, the gap is especially obvious. In practical engineering application, considering the time-varying characteristics of shotcrete will help to select the appropriate support setting time.

In this study, the calculation methods of the rock displacement at any distance from the excavation face and the supporting force of the subcomponents of the initial supporting structure are obtained, which makes up for the limitation of the traditional convergence constraint method applied to the supporting design, and can provide a reference for the tunnel supporting structure design.

Generally speaking, the shorter the time for shotcrete to reach the design strength, the better the ability to control rock deformation, but at the same time, the greater the load it bears. The selection of setting time of supporting structure should comprehensively consider the influence of rock displacement, time-varying characteristics of shotcrete, and tunnel tunneling rate. Through the calculation method of this study, the selection of support time can be optimized, and the ideal support effect can be achieved on the premise of ensuring support safety and rock stability.

This study can provide a new understanding for SRC, but the coupling change process of rock and supporting structure is not taken into account, which is worthy of further study in the future work.

Data Availability

The data used to support the findings of this study are included within the article.

Conflicts of Interest

The authors declare that there are no conflicts of interest regarding the publication of this article.

Acknowledgments

The research described in this study was funded by the National Key R&D Program of China (grant no. 2017YFC0805306), the National Nature Science Foundation of China (NSFC) (grant no. 51978059), and the Fundamental Research Funds for the Central Universities (grant no. 300102218517). These financial supports are gratefully acknowledged.

References

[1] L. Rabcewicz, "The new Austrian tunneling method. Part one, water power: 453–457 part two," *Water Power*, vol. 1, pp. 511–515, 1964.

[2] L. Müller, "Removing the misconceptions on the new Austrian tunneling method," *Tunnels Tunnelling*, vol. 22, pp. 15–18, 1990.

[3] J. Oke, *Determination of Nomenclature, Mechanistic Behavior, and Numerical Modelling Optimization of Umbrella Arch Systems*, Queen's University, Kingston, Canada, 2016.

[4] R. Fenner, "A study of ground pressure," *Gluckauf*, vol. 74, pp. 681–695, 1937.

[5] E. T. Brown, J. W. Bray, B. Ladanyi, and E. Hoek, "Ground response curves for rock tunnels," *Journal of Geotechnical Engineering*, vol. 109, no. 1, pp. 15–39, 1983.

[6] D. N. Minh, P. Habib, and Y. Guerpillon, *Time Dependent Behaviour of a Pilot Tunnel Driven in Hard Marls. Design and Performance of Underground Excavations*, ISRM/BGS, Cambridge, UK, 1984.

[7] C. Carranza-Tones and C. Fairhurst, "Application of the convergence-confinement method of tunnel design to rock masses that satisfy the Hoek-Brown failure criterion," *Tunnelling and Underground Space Technology*, vol. 15, no. 2, pp. 187–273, 2000.

[8] H. Fujimura, T. Nishimura, and Y. Ikezoe, "Theoretical construction of bearing characteristic curve in tunnelling," *Journal of the Society of Materials Science, Japan*, vol. 41, no. 463, pp. 417–423, 1992.

[9] C. Fairhurst and J. J. K. Deamen, "Practical inferences from research on the design of tunnel supports," *Underground Space*, vol. 4, pp. 297–311, 1980.

[10] J. Yamatomi, G. Mogi, and U. Yamaguchi, "Supporting effects of tunnel face," in *Proceedings of the 8th Japan Symposium on Rock Mechanics*, pp. 261–266, Tokyo, Japan, 1990.

[11] B. Ladanyi and D. E. Gill, "Design of tunnel linings in a creeping rock," *International Journal of Mining and Geological Engineering*, vol. 6, no. 2, pp. 113–126, 1988.

[12] I. D. Peila and I. P. P. Oreste, "Axisymmetric analysis of ground reinforcing in tunnelling design," *Computers and Geotechnics*, vol. 17, no. 2, pp. 253–274, 1995.

[13] R. R. Osgoui and P. Oreste, "Elasto-plastic analytical model for the design of grouted bolts in a Hoek-Brown medium," *International Journal for Numerical and Analytical Methods in Geomechanics*, vol. 34, no. 16, pp. 1651–1686, 2010.

[14] B. Indraratna and P. K. Kaiser, "Analytical model for the design of grouted rock bolts," *International Journal for Numerical and Analytical Methods in Geomechanics*, vol. 14, no. 4, pp. 227–251, 1990.

[15] H. Stille, M. Holmberg, and G. Nord, "Support of weak rock with grouted bolts and shotcrete," *International Journal of Rock Mechanics and Mining Sciences & Geomechanics Abstracts*, vol. 26, no. 1, pp. 99–113, 1989.

[16] A. Fahimifar and H. Soroush, "A theoretical approach for analysis of the interaction between grouted rockbolts and rock masses," *Tunnelling and Underground Space Technology*, vol. 20, no. 4, pp. 333–343, 2005.

[17] A. Bobet and H. H. Einstein, "Tunnel reinforcement with rockbolts," *Tunnelling and Underground Space Technology*, vol. 26, no. 1, pp. 100–123, 2011.

[18] Q. Fang, D. Zhang, P. Zhou, and L. N. Y. Wong, "Ground reaction curves for deep circular tunnels considering the effect of ground reinforcement," *International Journal of Rock Mechanics and Mining Sciences*, vol. 60, pp. 401–412, 2013.

[19] P. Li, F. Wang, and Q. Fang, "Undrained analysis of ground reaction curves for deep tunnels in saturated ground considering the effect of ground reinforcement," *Tunnelling and Underground Space Technology*, vol. 71, pp. 579–590, 2018.

[20] P. P. Oreste, "Analysis of structural interaction in tunnels using the covergence-confinement approach," *Tunnelling and Underground Space Technology*, vol. 18, no. 4, pp. 347–363, 2003.

[21] P. P. Oreste and D. Pella, "Modelling progressive hardening of shotcrete in convergence-confinement approach to tunnel design," *Tunnelling and Underground Space Technology*, vol. 12, no. 3, pp. 425–431, 1997.

[22] H. Stille and T. Franzen, "Design of shotcrete support from the rock mechanics viewpoint," in *Proceedings of the 1990 Engineering Foundation Conference-Shotcrete for Underground Support V*, Uppsala, Sweden, 1990.

[23] T. Zhang and W. Qin, "Tensile creep due to restraining stresses in high-strength concrete at early ages," *Cement Concrete Research*, vol. 36, no. 3, pp. 584–591, 2006.

[24] Y. Wei, S. Liang, W. Guo, and W. Hansen, "Stress prediction in very early-age concrete subject to restraint under varying temperature histories," *Cement and Concrete Composites*, vol. 83, pp. 45–56, 2017.

[25] K. Kolver, S. Igarashi, and A. Bentur, "Tensile creep behavior of high strength concretes at early ages," *Materials and Structures*, vol. 32, no. 5, pp. 383–387, 1999.

[26] M. Mazloom, "Estimating long-term creep and shrinkage of high-strength concrete," *Cement and Concrete Composites*, vol. 30, no. 4, pp. 316–326, 2008.

[27] Y. Wei, S. Liang, and W. Guo, "Decoupling of autogenous shrinkage and tensile creep strain in high strength concrete at early ages," *Experimental Mechanics*, vol. 57, no. 3, pp. 475–485, 2017.

[28] P. Chen, W. Zheng, Y. Wang, and W. Chang, "Creep model of high-strength concrete containing supplementary cementitious materials," *Construction and Building Materials*, vol. 202, pp. 494–506, 2019.

[29] E. K. Tschegg, A. Schneemayer, I. Merta, and K. A. Rieder, "Energy dissipation capacity of fibre reinforced concrete under biaxial tension-compression load. Part I: test equipment and work of fracture," *Cement and Concrete Composites*, vol. 62, pp. 195–203, 2015.

[30] J. Lee, S. Hong, C. Joh, I. Kwahk, and J. Lee, "Biaxial tension–compression strength behaviour of UHPFRC in-plane elements," *Materials and Structures*, vol. 50, no. 1, p. 20, 2017.

[31] J. M. F. Calixto, "Microcracking of high performance concrete subjected to biaxial tension—compression stresses," *Materials Research*, vol. 5, no. 3, pp. 295–299, 2002.

[32] L. Shen, L. Wang, Y. Song, and L. Shi, "Comparison between dynamic mechanical properties of dam and sieved concrete under biaxial tension-compression," *Construction and Building Materials*, vol. 132, pp. 43–50, 2017.

[33] P. L. Domone, "Uniaxial tensile creep and failure of concrete," *Magazine of Concrete Research*, vol. 26, no. 88, pp. 144–152, 1974.

[34] A. J. Babafemi and W. P. Boshoff, "Tensile creep of macro-synthetic fibre reinforced concrete (MSFRC) under uni-axial tensile loading," *Cement and Concrete Composites*, vol. 55, pp. 62–69, 2015.

[35] L. Vandewalle, "Concrete creep and shrinkage at cyclic ambient conditions," *Cement and Concrete Composites*, vol. 22, no. 3, pp. 201–208, 2000.

[36] F. Ghasemzadeh, A. Manafpour, S. Sajedi, M. Shekarchi, and M. Hatami, "Predicting long-term compressive creep of concrete using inverse analysis method," *Construction and Building Materials*, vol. 124, pp. 496–507, 2016.

[37] I. J. Jordaan and J. M. Illston, "The creep of sealed concrete under multiaxial compressive stresses," *Magazine of Concrete Research*, vol. 21, no. 69, pp. 195–204, 1969.

[38] L. Charpin, Y. Le Pape, É. Coustabeau et al., "A 12 year EDF study of concrete creep under uniaxial and biaxial loading," *Cement and Concrete Research*, vol. 103, pp. 140–159, 2018.

[39] S. Altoubat and D. Lange, "Creep, shrinkage, and cracking of restrained concrete at early age," *ACI Materials Journal*, vol. 98, no. 4, pp. 323–331, 2001.

[40] L. Østergaard, D. A. Lange, S. A. Altoubat, and H. Stang, "Tensile basic creep of early-age concrete under constant load," *Cement and Concrete Research*, vol. 31, no. 12, pp. 1895–1899, 2001.

[41] T. Heather, K. Emmanuel, and A. Matthew, "Shrinkage cracking characteristics of concrete using ring specimens," *ACI Materials Journal*, vol. 100, no. 3, pp. 239–245, 2003.

[42] Y. Gao, J. Zhang, and P. Han, "Determination of stress relaxation parameters of concrete in tension at early-age by ring test," *Construction and Building Materials*, vol. 41, pp. 152–164, 2013.

[43] N. Ranaivomanana, S. Multon, and A. Turatsinze, "Tensile, compressive and flexural basic creep of concrete at different stress levels," *Cement and Concrete Research*, vol. 52, pp. 1–10, 2013.

[44] S. Liang and Y. Wei, "Methodology of obtaining intrinsic creep property of concrete by flexural deflection test," *Cement and Concrete Composites*, vol. 97, pp. 288–299, 2019.

[45] K. S. Gopalakrishnan, A. M. Neville, and A. Ghali, "Creep Poisson's ratio of concrete under multiaxial compression," *ACI Journal Proceedings*, vol. 66, no. 12, pp. 1008–1019, 1969.

[46] L. H. Ichinose, E. Watanabe, and H. Nakai, "An experimental study on creep of concrete filled steel pipes," *Journal of Constructional Steel Research*, vol. 57, no. 4, pp. 453–466, 2001.

[47] M. Ke, H. Liu, H. Liu, and S. Chen, "Biaxial creep experiment for high strength concrete in bridge engineering," *Journal of Building Structures*, vol. 33, no. 6, pp. 116–122, 2012, in Chinese.

[48] ACI Committee 209, *Prediction of Creep Shrinkage, and Temperature Effects in Concrete Structures (AC1209R-82). Part 1*, Amercian Concrete Institute, Indianapolis, IN, USA, 1982.

[49] ACI Committee 209, *Prediction of Creep Shrinkage, and Temperature Effects in Concrete Structures (AC1209R-92). Part 1*, Amercian Concrete Institue, Indianapolis, IN, USA, 1992.

[50] N. J. Gardner and M. J. Lockman, "Design provisions for dying shrinkage and creep of normal strength concrete," *ACI Materials Journal*, vol. 98, no. 2, pp. 159–167, 2001.

[51] CEB-FIP, *Model Code for Concrete Structures*, CEB-FIP International Recommendations, Paris, France, 1978.

[52] Z. P. Bazant and L. Panula, "Creep and shrinkage characterization for analyzing prestressed concrete structures," *PCI Journal*, vol. 25, no. 3, p. 86122, 1980.

[53] Z. P. Bazant, "Prediction of concrete creep effects using age-adjusted effective modulus method," *ACI Materials Journal*, vol. 69, pp. 212–217, 1972.

[54] N. J. Gardner and J. W. Zhao, "Creep and shrinkage revisited," *ACI Materials Journal*, vol. 90, no. 3, pp. 236–246, 1993.

[55] R. Goel, R. Kumar, and S. P. D. K. Paul, "Comparative study of various creep and shrinkage prediction models for concrete," *Journal of Materials in Civil Engineering*, vol. 19, no. 3, pp. 249–260, 2007.

[56] J. P. Lam, *Evaluation of Concrete Shrinkage and Creep Prediction Models*, San José State University, San Jose, CA, USA, 2002.

[57] D. W. Mokarem, *Development of Concrete Shrinkage Performance Specifications*, Virginia Polytechnic Institute and State University, Blacksburg, VA, USA, 2002.

[58] A. M. Neville, W. H. Dilger, and J. J. Brooks, *Creep of Plain and Structural Concrete*, Construction Press, London, UK, 1982.

[59] A. M. Akthem and J. P. Lam, "Statistical evaluation of shrinkage and creep models," *ACI Material Journal Technical Papers*, vol. 102, no. 3, 170 pages, 2005.

[60] J. A. Bay and K. H. Stokoe II, "Field determination of stiffness and integrity of PCC members using the SASW method," in *Proceedings of the Nondestructive Evaluation of Civil Structures and Materials Conference*, pp. 71–86, Boulder, CO, USA, 1990.

[61] Y.-W. Pan and J.-J. Dong, "Time-dependent tunnel convergence-I. Formulation of the model," *International Journal of Rock Mechanics and Mining Sciences & Geomechanics Abstracts*, vol. 28, no. 6, pp. 469–475, 1991.

[62] M. K. Rahman, M. H. Baluch, and A. H. A1-Gadhib, "Simulation of shrinkage distress and creep relief in concrete repair," *Composites Part B: Engineering*, vol. 31, no. 6-7, pp. 541–553, 2000.

[63] Z.-F. Al-Gadhib, S.-L. Shen, G. Modoni, and A. Zhou, "Excess pore water pressure caused by the installation of jet grouting columns in clay," *Computers and Geotechnics*, vol. 125, Article ID 103667, 2020.

[64] J. Qiu, H. Liu, J. Lai, H. Lai, J. Chen, and K. Wang, "Investigating the long-term settlement of a tunnel built over improved loessial foundation soil using jet grouting technique," *Journal of Performance of Constructed Facilities*, vol. 32, no. 5, Article ID 04018066, 2018.

[65] J. Qiu, Y. Xie, H. Fan, Z. Wang, and Y. Zhang, "Centrifuge modelling of twin-tunnelling induced ground movements in loess strata," *Arabian Journal of Geosciences*, vol. 10, no. 22, p. 493, 2017.

[66] J. Lai, H. Fan, J. Chen, J. Qiu, and K. Wang, "Blasting vibration monitoring of undercrossing railway tunnel using wireless sensor network," *International Journal of Distributed Sensor Networks*, vol. 11, no. 6, Article ID 703980, 2015.

[67] J. Lai, X. Wang, J. Qiu et al., "A state-of-the-art review of sustainable energy based freeze proof technology for cold-region tunnels in China," *Renewable and Sustainable Energy Reviews*, vol. 82, no. 3, pp. 3554–3569, 2017.

[68] P. Li, K. Chen, F. Wang, and Z. Li, "An upper-bound analytical model of blow-out for a shallow tunnel in sand considering the partial failure within the face," *Tunnelling and Underground Space Technology*, vol. 91, Article ID 102989, 2019.

[69] Y.-q. Wang, S. Xu, R. Ren, S. Zhang, and Z. Ren, "Application of the twin-tube complementary ventilation system in large-slopping road tunnels in China," *International Journal of Ventilation*, vol. 19, no. 1, pp. 63–82, 2020.

[70] J. Sun and H. H. Zhu, "Mechanical simulation and analysis of behavior of soft and weak rocks in the construction of a tunnel opening," *Rock and Soil Mechanics*, vol. 15, no. 4, pp. 20–23, 1994, in Chinese.

[71] M. Panel, "Analysis of convergence behind the face of a tunnel," in *Proceedings of the 3rd International Symposium*, Brighton, UK, June 1982.

[72] B. G. Liu and X. D. Du, "Visco-elastical analysis on interaction between supporting structure and surrounding rocks of circle Tunnel," *Chinese Journal of Rock Mechanics and Engineering*, vol. 23, no. 4, p. 561, 2004.

[73] N. Vlachopoulos and M. S. Diederichs, "Improved longitudinal displacement profiles for convergence confinement analysis of deep tunnels," *Rock Mechanics and Rock Engineering*, vol. 42, no. 2, pp. 131–146, 2009.

[74] L. R. Alejano, A. Rodríguez-Dono, M. Veiga, and M. Veiga, "Plastic radii and longitudinal deformation profiles of tunnels excavated in strain-softening rock masses," *Tunnelling and Underground Space Technology*, vol. 30, no. 1, pp. 169–182, 2012.

[75] E. Hoek and E. T. Brown, *Underground Excavations in Rock*, The Institution of Mining and Metallurgy, London, UK, 1980.

[76] L. F. Zhang, *Research and Software Development on Creep Contraction and Prestress of Bridge Structures*, Chang'an University, Xi'an, China, 2002, in Chinese.